Measurements of the separated longitudinal structure function F_L from hydrogen and deuterium targets at low Q^2

V. Tvaskis,[1] A. Tvaskis,[1] I. Niculescu,[2] D. Abbott,[3] G. S. Adams,[4] A. Afanasev,[3] A. Ahmidouch,[5] T. Angelescu,[6] J. Arrington,[7] R. Asaturyan,[8] S. Avery,[1] O. K. Baker,[1,3] N. Benmouna,[9] B. L. Berman,[9] A. Biselli,[10] H. P. Blok,[11,12] W. U. Boeglin,[13] P. E. Bosted,[3,14] E. Brash,[15] H. Breuer,[16] G. Chang,[16] N. Chant,[16] M. E. Christy,[1] S. H. Connell,[17] M. M. Dalton,[18] S. Danagoulian,[5] D. Day,[18] T. Dodario,[19] J. A. Dunne,[20] D. Dutta,[21] N. El Khayari,[19] R. Ent,[3] H. C. Fenker,[3] V. V. Frolov,[22] D. Gaskell,[3] K. Garrow,[23] R. Gilman,[24] P. Gueye,[1] K. Hafidi,[7] W. Hinton,[1] R. J. Holt,[7] T. Horn,[3] G. M. Huber,[15] H. Jackson,[7] X. Jiang,[24] M. K. Jones,[3] K. Joo,[25] J. J. Kelly,[16] C. E. Keppel,[3] J. Kuhn,[10] E. Kinney,[26] A. Klein,[27] V. Kubarovsky,[3] Y. Liang,[28] G. Lolos,[15] A. Lung,[3] D. Mack,[3] S. Malace,[1] P. Markowitz,[13] G. Mbianda,[18] E. McGrath,[2] D. Mckee,[29] D. G. Meekins,[3] H. Mkrtchyan,[8] J. Napolitano,[4] T. Navasardyan,[8] G. Niculescu,[2] M. Nozar,[3] T. Ostapenko,[30] Z. Papandreou,[15] D. Potterveld,[7] P. E. Reimer,[7] J. Reinhold,[13] J. Roche,[3] S. E. Rock,[14] E. Schulte,[7] E. Segbefia,[1] C. Smith,[18] G. R. Smith,[3] P. Stoler,[4] V. Tadevosyan,[8] L. Tang,[1,3] J. Telfeyan,[2] L. Todor,[10] M. Ungaro,[4] A. Uzzle,[1] S. Vidakovic,[15] A. Villano,[4] W. F. Vulcan,[3] G. Warren,[3] F. Wesselmann,[18] B. Wojtsekhowski,[3] S. A. Wood,[3] C. Yan,[3] and B. Zihlmann[3]

[1]*Hampton University, Hampton, Virginia 23668, USA*
[2]*James Madison University, Harrisonburg, Virginia 22807, USA*
[3]*Physics Division, Thomas Jefferson National Accelerator Facility, Newport News, Virginia 23606, USA*
[4]*Rensselaer Polytechnic Institute, Troy, New York 12180, USA*
[5]*North Carolina A & T State University, Greensboro, North Carolina 27411, USA*
[6]*Faculty of Physics, Bucharest University, Magurele, 077125, Romania*
[7]*Physics Division, Argonne National Laboratory, Argonne, Illinois 60439, USA*
[8]*Yerevan Physics Institute, 375036 Yerevan, Armenia*
[9]*The George Washington University, Washington, D.C. 20052, USA*
[10]*Carnegie Mellon University, Pittsburgh, Pennsylvania 15213, USA*
[11]*Vrije University, 1081 HV Amsterdam, The Netherlands*
[12]*Nikhef, 1009 DB Amsterdam, The Netherlands*
[13]*Florida International University, University Park, Florida 33199, USA*
[14]*University of Massachusetts Amherst, Amherst, Massachusetts 01003, USA*
[15]*University of Regina, Regina, Saskatchewan, Canada S4S 0A2*
[16]*University of Maryland, College Park, Maryland 20742, USA*
[17]*University of the Witwatersrand, Johannesburg 2000, South Africa*
[18]*University of Virginia, Charlottesville, Virginia 22901, USA*
[19]*University of Houston, Houston, Texas 77204, USA*
[20]*Mississippi State University, Mississippi State, Mississippi 39762, USA*
[21]*Triangle Universities Nuclear Laboratory and Duke University, Durham, North Carolina 27708, USA*
[22]*California Institute of Technology, Pasadena, California 91125, USA*
[23]*University of Saskatchewan, Saskatoon, Saskatchewan, Canada S7N 5A3*
[24]*Rutgers, The State University of New Jersey, Piscataway, New Jersey 08855, USA*
[25]*University of Connecticut, Storrs, Connecticut 06269, USA*
[26]*University of Colorado, Boulder, Colorado 80309, USA*
[27]*Old Dominion University, Norfolk, Virginia 23529, USA*
[28]*Ohio University, Athens, Ohio 45071, USA*
[29]*Arizona State University, Tempe, Arizona 85287, USA*
[30]*Gettysburg College, Gettysburg, Pennsylvania 18103, USA*

Structure functions, as measured in lepton-nucleon scattering, have proven to be very useful in studying the partonic dynamics within the nucleon. However, it is experimentally difficult to separately determine the longitudinal and transverse structure functions, and consequently there are substantially less data available in particular for the longitudinal structure function. Here, we present separated structure functions for hydrogen and deuterium at low four-momentum transfer squared, $Q^2 < 1 \, \text{GeV}^2$, and compare them with parton distribution parametrization and k_T factorization approaches. While differences are found, the parametrizations generally agree with the data, even at the very low-Q^2 scale of the data. The deuterium data show a smaller longitudinal structure function and a smaller ratio of longitudinal to transverse cross section, R, than the proton. This suggests

either an unexpected difference in R for the proton and the neutron or a suppression of the gluonic distribution in nuclei.

I. INTRODUCTION

Nucleon and nuclear structure functions, as measured in inclusive electron scattering, have proven to be very useful in probing the fundamental, underlying quark dynamics. Lepton-nucleon scattering experiments at high energy have been conducted over a wide kinematic range at various experimental facilities such as SLAC, DESY, CERN, and Jefferson Lab (see Refs. [1–7]). The data obtained from these experiments have helped develop the description of hadrons as composite objects of quarks and gluons which interact weakly at high-energy scales, but very strongly at low-energy scales. At large enough values of the square of the four-momentum transfer, Q^2 ($Q^2 = -q^2$, the virtuality of the photon), corresponding to small wavelengths of the virtual photon probe, the lepton-nucleon interaction can be viewed as the incoherent scattering of the virtual photon from a single quark. The experimental results can be interpreted in the framework of perturbative QCD in terms of single-parton densities. However, as Q^2 decreases, the description of the nucleon's structure becomes more complex, and initial and final state interactions between the struck quark and the remnants of the target must be included. The transition from perturbative to nonperturbative QCD is of great interest as it involves the fundamental dynamics of strongly bound matter, which are not yet well understood.

The kinematics for the inclusive electron-proton scattering process can be described in the one-photon exchange approximation in terms of Q^2 and the Bjorken scaling variable $x = Q^2/2M\nu$, where $\nu = E - E'$ is the energy of the virtual photon exchanged in the target rest frame, M is the proton mass, and E and E' are the incident and scattered electron energies, respectively. In this case, the differential cross section for inclusive unpolarized electron scattering can be written as

$$\frac{1}{\Gamma}\frac{d^2\sigma}{d\Omega\, dE'} = \sigma_T + \varepsilon\sigma_L. \tag{1}$$

Here σ_L and σ_T are the longitudinal and transverse virtual photon absorption cross sections, respectively, and Γ is the transverse virtual photon flux factor,

$$\Gamma = \frac{\alpha}{2\pi^2 Q^2}\frac{E'}{E}\frac{1}{1-\varepsilon}. \tag{2}$$

Here, ε is the relative longitudinal virtual photon polarization and α is the fine-structure constant:

$$\varepsilon = \left[1 + 2\left(1 + \frac{\nu^2}{Q^2}\right)\tan^2\left(\frac{\theta}{2}\right)\right]^{-1}. \tag{3}$$

It is convenient to define two dimensionless structure functions, F_1 and F_2, which are related to σ_L and σ_T, as follows:

$$F_1(x, Q^2) = \frac{Q^2}{4\pi^2\alpha}\frac{(1-x)}{2x}\sigma_T, \tag{4}$$

$$F_2(x, Q^2) = \frac{Q^2}{4\pi^2\alpha}\frac{1}{1 + \frac{Q^2}{\nu^2}}(1-x)(\sigma_L + \sigma_T). \tag{5}$$

The F_1 structure function depends only on the transverse virtual absorption cross section and is therefore sensitive in perturbative quantum chromodynamics (pQCD) to single-parton densities. The more commonly used F_2 is a linear combination of both longitudinal and transverse couplings. A purely longitudinal structure function can be defined as

$$F_L(x, Q^2) = \frac{Q^2}{4\pi^2\alpha}(1-x)\sigma_L. \tag{6}$$

In the naive parton model this longitudinal structure function is correlated with the average transverse momentum of the partons. In a QCD collinear framework at next-to-leading-order, F_L is interpreted in terms of the gluon distribution inside the nucleon [8] and can be written in terms of the gluon density $G(x, Q^2)$ using the Altarelli-Martinelli equation [9]:

$$F_L(x, Q^2) = \frac{\alpha}{\pi}\left[\frac{4}{3}\int_x^1 \frac{dy}{y}\left(\frac{x}{y}\right)^2 F_2(y, Q^2)\right.$$
$$\left. + 2\sum_q e_q^2 \int_x^1 \frac{dy}{y}\left(\frac{x}{y}\right)^2\left(1 - \frac{x}{y}\right)G(y, Q^2)\right]. \tag{7}$$

At low x, theoretical models predict a dramatic increase in F_L due at least in part to gluon and quark-antiquark emission. Recent measurements of the longitudinal structure function from the H1 and ZEUS experiments at HERA [5,6] show a nonzero value for F_L at Bjorken $x \leqslant 0.007$ and large four-momentum transfer squared ($Q^2 \geqslant 20\,\text{GeV}^2$). These results have sparked renewed theoretical and experimental interest in this structure function (see, for example, Refs. [10–15]).

Typically, the ratio of longitudinal and transverse virtual photon absorption cross sections, R, is measured to determine F_L. R is defined as

$$R(x, Q^2) = \frac{\sigma_L}{\sigma_T} = \frac{F_L}{2xF_1}. \tag{8}$$

For scattering from spin-1/2 pointlike partons this ratio is expected to vanish at large Q^2 and moderate x, but is nonzero (of the order of 0.1 to 0.3 [16]) at low values of Q^2 and moderate x. This effect is due in part to the fact that in the naive parton model quarks can carry transverse momentum.

Determining separately the longitudinal and transverse structure functions, F_L and F_1, and thus the ratio R, is experimentally challenging. It may be achieved via a Rosenbluth-type separation technique [17] using Eq. (1). This procedure requires high-precision cross-section measurements at the same x and Q^2, but different values of ε, which requires in turn measurements at a minimum of two different incident beam energies and scattering angles [18]. Consequently, there are far fewer experimental data available for F_L, F_1, and R than for the structure function F_2.

Measured separated structure functions for the neutron, usually extracted from deuterium data due to the lack of a
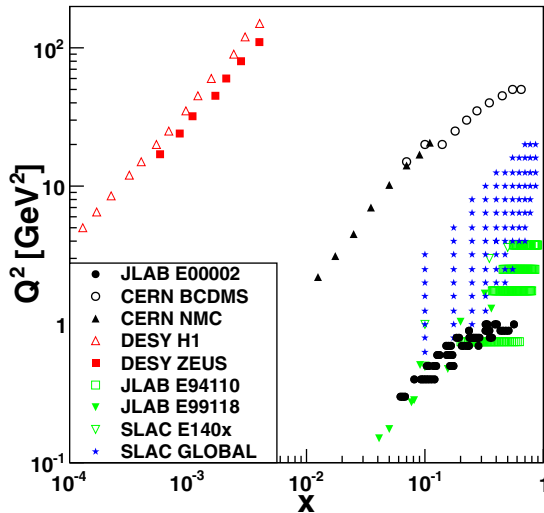
FIG. 1. Kinematic coverage of world data for the hydrogen longitudinal structure function: CERN BCDMS [3], open circles; CERN NMC [4], solid triangles; DESY H1 [5], open triangles; Jefferson Lab E94–110 [18], open squares; Jefferson Lab E99–118 [7], inverted solid triangles; SLAC E140X [2], inverted open triangles; SLAC GLOBAL [23], stars; and Jefferson Lab E00–002 (current experiment), solid circles.

free neutron target, are even fewer than those for hydrogen. Most of the existing deuterium measurements were performed at large four-momentum transfer and do not show significant differences compared to hydrogen [1,2]. This could be due, however, to R itself being quite small at these kinematics, such that any differences may be buried in the measurement uncertainties. Measurements of R at Jefferson Lab [7] in the low-Q^2 regime, where R is larger and differences may appear, show a slight difference between hydrogen and deuterium. This is somewhat unexpected, but not in contradiction with theoretical predictions. There is no requirement in pQCD for R to be the same for the proton and the neutron. While hadron helicity conservation requires that both must go to zero at large Q^2, there is no requirement that finite-Q^2 corrections or values be identical. However, it is generally assumed that $R_p = R_d$ and that higher-twist corrections are identical, e.g., in the extraction of the neutron structure function F_2 from measurements on the deuteron and the proton [19–22]. It is equally doubtful that a partonic interpretation remains valid in the low-Q^2 nonperturbative regime.

In this article, we present results for F_L and R for the proton and deuteron at low values of Q^2 and intermediate x. The kinematic coverage of this experiment (JLab E00–002) is shown in Fig. 1 together with the coverage of world data: CERN [3,4], DESY [5,6], Jefferson Lab [7,18], and SLAC [2,23]. The present data extend the kinematic range in x at fixed low Q^2 to allow for more detailed studies of the x dependence, as well as for more deuteron and proton comparisons.

This article is structured in five sections. Sections II and III summarize the experiment and data analysis. Section IV discusses the longitudinal structure function results for

hydrogen, while Sec. V presents the comparison of the hydrogen and deuterium structure functions. Conclusions are drawn in Sec. VI.

II. EXPERIMENT

Experiment E00–002 was carried out in Hall C at the Thomas Jefferson National Accelerator Facility (Jefferson Lab or JLab). The experiment utilized the high-luminosity, continuous-wave electron beam provided by the Continuous Electron Beam Accelerator Facility (CEBAF). The kinematic range covered was $0.2 < Q^2 < 1.1 \text{ GeV}^2$ and $0.02 < x < 0.6$. Electron-proton and electron-deuteron cross sections were measured using four incident electron beam energies (2.24, 3.04, 4.41, and 5.50 GeV). To minimize systematic uncertainties, the beam current was kept within a few microamperes of the 20 μA nominal value.

The cryogenic targets used were 4-cm-long hydrogen (H) and deuterium (D) "tuna can"-shaped aluminum cells of 0.125 mm in thickness. The target assembly, described in detail in Refs. [24,25], also included an aluminum "dummy target" that was used for background measurements and subtraction. Precise cross-section measurements require accurate knowledge of target thickness and target density. Due to the circular geometry of the cryogenic target cell, the effective target length seen by the beam depended upon both the central position of the beam spot and the size and form of the beam raster pattern. The effective target length, determined for Jefferson Lab experiment E00–116, which ran during the same period, is presented in Ref. [24]. Density fluctuation studies for the target cells and the beam currents used in this experiment are presented in Refs. [24,25] and amount to 0.35%/100 μA.

The basic equipment in Hall C at Jefferson Lab consists of two magnetic spectrometers: the high momentum spectrometer (HMS) and the short orbit spectrometer (SOS). HMS is a magnetic spectrometer consisting of a 25° vertical bend dipole magnet for momentum dispersion and three quadrupole magnets for focusing. For this experiment, the HMS was operated in point-to-point optical tune. The HMS solid angle is defined mainly by the octagonal collimator and is 6.8 msr. The HMS momentum acceptance is ±8%, while the angular acceptance is ±35 mrad. The SOS was a resistive $QD\bar{D}$ magnetic spectrometer with a 9 msr solid angle. The SOS momentum acceptance was −15% to +20%, while the scattering angle acceptance was ±60 mrad.

The HMS and SOS detector packages were very similar, consisting of two drift chambers for track reconstruction (the HMS drift chambers are described in Ref. [26]), scintillator arrays for triggering, and a threshold gas Čerenkov and electromagnetic calorimeters [27], which were both used for particle identification and pion rejection. More details on the two spectrometers and their detector packages can be found in Refs. [24,28–31].

The HMS was used to detect the scattered electrons, while the SOS was used for detecting positrons needed to estimate the electron background originating from charge-symmetric processes, such as π^0 production and subsequent pair

symmetric decay. The data were taken at HMS angles varying from 11° to 50°.

III. DATA ANALYSIS

The inclusive double-differential cross section for each energy and angle bin within the spectrometer acceptance was determined from

$$\frac{d\sigma}{d\Omega dE'} = \frac{Y_{\text{corr}}}{L\Delta\Omega\Delta E'}, \tag{9}$$

where $\Delta\Omega(\Delta E')$ is the bin width in solid angle (scattered electron energy), L is the total integrated luminosity, and Y_{corr} is the measured electron yield after accounting for detector inefficiencies, background events mentioned above, and radiative corrections.

In a closed geometry spectrometer such as the HMS or SOS, neither the forward-peaked bremsstrahlung photons emitted from scattered electrons nor their very low-energy secondaries from pair conversion in materials upstream of the magnets are detected due to the upward bend of the momentum-resolving dipole field. Additionally, secondaries produced in the detector hut from the emission of hard photons associated with nuclear elastic scattering off the deuteron are easily isolated based on reconstructed trajectories that do not correspond to those transported though the magnetic system. No evidence has been found that these impact the efficiency of the various detector systems. This is quite different from the case of open geometry spectrometers such as HERMES [32]. Hence, the primary effect of the bremsstrahlung emission is to modify the measured momentum from that at the scattering vertex.

To obtain the Born cross section (the leading-order, one-photon-exchange contribution), the measured yield has to be corrected for the higher-order electromagnetic processes that contribute to inclusive electron-nucleon scattering. These radiative processes can be divided into two main categories: internal, which originate due to the fields of the particles at the scattering vertex (vacuum polarization, vertex corrections, two-photon exchange, and bremsstrahlung emission in the field of the proton from which the scattering took place), and external, which originate due to the fields of particles in the bulk target materials (processes that occur either before or after the primary scattering vertex). The radiative correction factors, which account for these higher-order processes, were evaluated using the same procedure as Refs. [24,25]. The procedure utilized the prescription of Mo and Tsai [33,34] for the external and the more exact prescription of Bardin *et al.* [35] for the internal, as described in Refs. [1,36]. The theoretical uncertainties in the radiative correction procedure were studied in Ref. [37] and were estimated to be 0.5% point-to-point and 1.0% normalized.

A bin-centering correction, to account for the variation of the cross section over the angular acceptance, and a radiative effects correction were applied to every bin in scattering angle θ and scattered electron energy. The radiative effects strongly depend on the kinematics. An iterative procedure was

TABLE I. Summary of systematic uncertainties in the differential cross section.

Quantity	Uncertainty
Beam energy	0.30%
Scattered electron energy	0.25%
Scattered electron angle	0.30%
Beam charge	0.71–1.07%
Target density	0.35%
Dead-time corrections	0.25%
Tracking efficiency	0.25%
Efficiency (Cer. cal.)	0.35%
Charge symmetric background	0.20%
Bin centering	0.5%
Acceptance correction	0.50%
Radiative corrections, normalization	1.0%
Radiative corrections, point-to-point	0.50%
Total (not including radiative corrections)	1.29–1.51%

employed to minimize the dependence on the model [38,39] used to compute both the bin-centering and the radiative effects corrections. Corrected data were fit to obtain new parameters for the model used, new corrections were calculated, and the steps were repeated until the fit parameters converged. The bin-centering correction uncertainty was estimated to be about 0.5% for the kinematics of these data.

The total systematic uncertainty in the differential cross section was taken as the quadratic sum of all contributing systematic uncertainties. Excluding the radiative correction uncertainty, the total systematic uncertainty was 1.29% and 1.51% per kinematic bin (see Table I).

The extraction of the longitudinal structure function was accomplished via the Rosenbluth technique, where measurements are made for two or more values of ϵ at fixed Bjorken x and Q^2, and the reduced cross section is fit linearly as a function of ϵ, as in Eq. (1). Because the corrected data at various ϵ are not at the exactly same x and Q^2 as needed for the Rosenbluth separation method, the data were interpolated to common x and Q^2 using a parametrization of the cross section [38,39]. Figure 2 shows four representative Rosenbluth separations from the deuterium data set. The quantity shown is the reduced cross section defined as

$$\sigma_T + \epsilon\sigma_L = \frac{4\pi^2\alpha}{Q^2}\frac{2x}{(1-x)}\left[F_1 + \frac{\epsilon}{2x}F_L\right]. \tag{10}$$

In a Rosenbluth separation, one needs to distinguish between uncertainties that are correlated between measurements at different ϵ, such as uncertainties in target thickness and integrated charge, and uncorrelated ones, such as spectrometer acceptance or background subtraction at different angles. Not including the contributions from radiative corrections, the uncorrelated systematic uncertainties in the cross-section measurements were ∼0.88%.

Both Γ and ϵ were calculated from the measured kinematic variables using Eqs. (2) and (3), respectively. The intercept of the fit is the transverse cross section σ_T [and therefore the
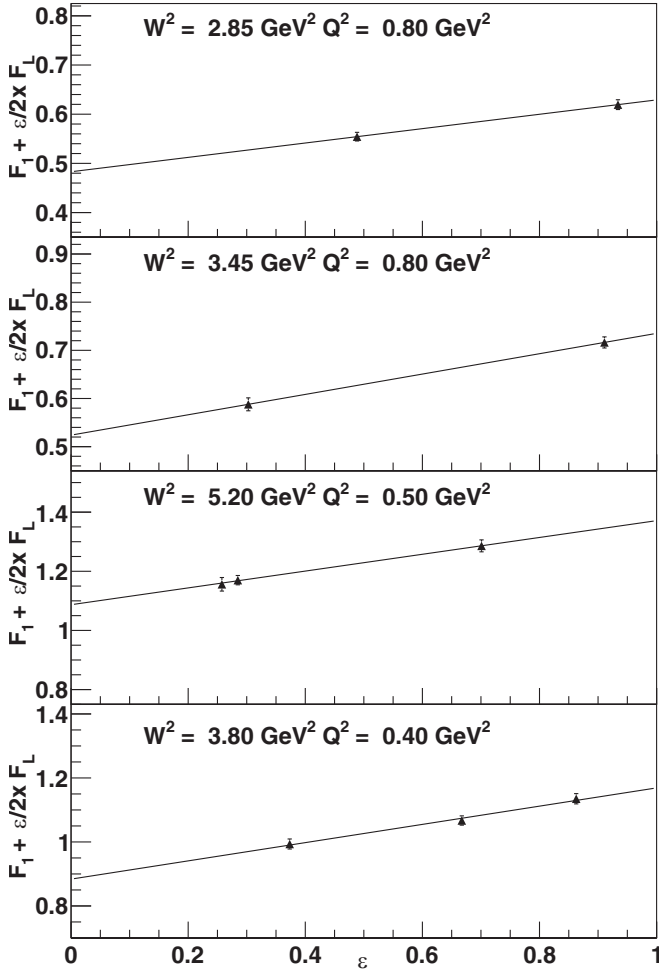
FIG. 2. Rosenbluth separation for four (Q^2, W^2) deuterium points. The quantity plotted on the vertical axis is $F_1 + (\epsilon/2x)F_L$ as described in Eq. (10).

FIG. 3. F_2 structure-function data for the proton as a function of the invariant mass squared, W^2. The three panels correspond to three different Q^2 regions: $Q^2 = 0.3\,\mathrm{GeV}^2$ (top panel), $Q^2 = 0.7\,\mathrm{GeV}^2$ (middle panel), and $Q^2 = 1.1\,\mathrm{GeV}^2$ (bottom panel). The data are compared with the Bosted-Christy (BC) parametrization [38] (solid curve).

IV. PROTON LONGITUDINAL STRUCTURE FUNCTION

The data were used to extract the proton F_2 structure function, as well as the proton longitudinal structure function F_L. Three representative spectra depicting the F_2 structure function, as a function of the invariant mass squared, W^2, are shown in Fig. 3. The data are compared with the Bosted-Christy (BC) parametrization [38], an empirical fit of inelastic electron-proton cross sections in the resonance region. The agreement between the data and this global fit is very good.

The results for the proton F_2 structure function, the longitudinal structure function F_L, and the ratio R are presented in Table II. The proton longitudinal structure function F_L is shown in Fig. 4 as a function of Bjorken x (for $x > 0.01$) for four different Q^2 regions: $Q^2 = 0.30$, 0.50, 0.80, and $1.0\,\mathrm{GeV}^2$. The data included are from this experiment, JLab experiment E99–118 [7], SLAC experiment E140X [2], and a global analysis of SLAC data [23]. At these low values of Q^2, there are no other separated data within this range of x, as can be seen from Fig. 1. The results for the deuteron differ from those for the proton and are discussed in Sec. IV.

The curves in Fig. 4 represent the ABKM parameterization [50,51] (solid and dotted black lines, adding respectively target mass and higher twist), the HERAPDF1.5 NNLO QCD global parton distribution (PDF) fit (solid green line) [52], and two k_T factorization (dashed-dotted and dashed red lines) parametrizations [12,53]. These calculations are shown only for the two higher-Q^2 values ($Q^2 = 0.8$ and $Q^2 = 1.0\,\mathrm{GeV}^2$), where the parametrizations become better constrained by existing structure function data. It should be noted that this is still below the region of validity for these models.

The ABKM parametrization is a next-to-next-to-leading-order (NNLO) PDF fit, obtained by a global analysis of available hard-scattering data in the $\overline{MS}$ factorization scheme. The ABKM parametrization of the structure function includes terms that take into account nonperturbative target-mass

structure function $F_1(x, Q^2)$], while the slope is the longitudinal cross section σ_L, from which the structure function $F_L(x, Q^2)$ can be calculated using Eq. (6).

The radiative corrections do not include the contribution of hard two-photon exchange (TPE). While this appears to have a significant impact on Rosenbluth extractions of G_E^p/G_M^p for electron-proton elastic scattering at high Q^2 [40–43], calculations and recent data suggest that they are typically below 1% for elastic scattering at the Q^2 values of this measurement [40,44–47]. Estimates of the TPE contribution to resonance production [48,49] suggest that the corrections for the resonance region are smaller than those for elastic scattering by roughly a factor of 2 for Δ production.

For the present data, the longitudinal cross section is typically 20–50% of the total cross section, so a change in the slope of $\leqslant 1\%$ would translate into a 2–5% correction to σ_L. Even though a definitive calculation of the two-photon effect is not available, this correction is typically smaller than the total statistical and systematic uncertainties and thus should have minimal impact on the final results. F_L is only sensitive to nonlinearities caused by the effect.
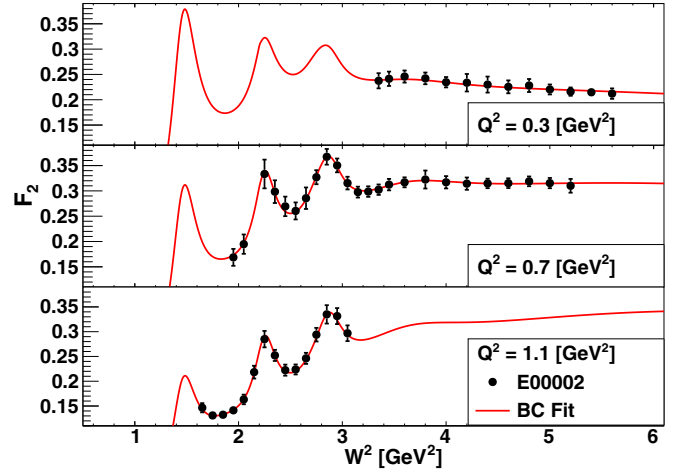
TABLE II. Proton structure functions R, F_2, and F_L extracted using the Rosebluth separation technique.

| Q^2 (GeV^2)	x	R	Δ_{stat}	Δ_{total}	F_2	Δ_{stat}	Δ_{total}	F_L	Δ_{stat}	Δ_{total}
0.30	0.062	0.2437	0.0757	0.0843	0.2178	0.0135	0.0148	0.0446	0.0123	0.0135
0.30	0.065	0.2418	0.0681	0.0739	0.2178	0.0120	0.0135	0.0445	0.0113	0.0121
0.30	0.068	0.2803	0.0788	0.0831	0.2235	0.0137	0.0150	0.0516	0.0126	0.0133
0.40	0.081	0.2037	0.0656	0.0724	0.2481	0.0139	0.0156	0.0444	0.0130	0.0141
0.40	0.093	0.3420	0.0804	0.0823	0.2650	0.0153	0.0171	0.0727	0.0144	0.0148
0.40	0.097	0.3005	0.0992	0.1003	0.2621	0.0201	0.0215	0.0656	0.0181	0.0183
0.40	0.102	0.3154	0.0915	0.0926	0.2657	0.0183	0.0198	0.0696	0.0168	0.0171
0.40	0.108	0.3665	0.1258	0.1266	0.2695	0.0242	0.0254	0.0797	0.0217	0.0219
0.40	0.114	0.3302	0.1313	0.1319	0.2692	0.0266	0.0277	0.0744	0.0238	0.0240
0.40	0.121	0.3441	0.0672	0.0697	0.2778	0.0137	0.0158	0.0802	0.0129	0.0135
0.50	0.104	0.2271	0.0564	0.0608	0.2768	0.0128	0.0151	0.0551	0.0125	0.0133
0.50	0.108	0.2149	0.0650	0.0674	0.2766	0.0152	0.0171	0.0530	0.0145	0.0149
0.50	0.119	0.2283	0.0868	0.0883	0.2819	0.0205	0.0221	0.0576	0.0193	0.0196
0.50	0.124	0.3303	0.1010	0.1020	0.2912	0.0217	0.0232	0.0802	0.0204	0.0206
0.50	0.163	0.4154	0.0909	0.0919	0.2933	0.0180	0.0198	0.1022	0.0175	0.0179
0.50	0.168	0.2891	0.0926	0.0932	0.2830	0.0205	0.0221	0.0761	0.0207	0.0209
0.50	0.174	0.2616	0.0828	0.0834	0.2835	0.0194	0.0210	0.0714	0.0191	0.0193
0.60	0.127	0.3225	0.0551	0.0575	0.3042	0.0126	0.0153	0.0812	0.0117	0.0122
0.60	0.133	0.3206	0.0569	0.0589	0.3095	0.0132	0.0158	0.0829	0.0124	0.0129
0.60	0.153	0.3329	0.1076	0.1083	0.3070	0.0244	0.0259	0.0872	0.0232	0.0234
0.60	0.161	0.4497	0.1303	0.1309	0.3129	0.0261	0.0276	0.1119	0.0249	0.0251
0.60	0.171	0.5026	0.1446	0.1452	0.3209	0.0279	0.0293	0.1256	0.0270	0.0272
0.70	0.152	0.3214	0.0652	0.0671	0.3185	0.0154	0.0178	0.0864	0.0150	0.0155
0.70	0.158	0.2303	0.0495	0.0511	0.3142	0.0133	0.0160	0.0662	0.0124	0.0128
0.70	0.166	0.2741	0.0550	0.0560	0.3131	0.0139	0.0165	0.0767	0.0131	0.0134
0.70	0.205	0.3283	0.0715	0.0731	0.3120	0.0163	0.0186	0.0934	0.0174	0.0179
0.70	0.214	0.5300	0.2343	0.2346	0.3156	0.0431	0.0440	0.1345	0.0433	0.0435
0.70	0.228	0.3642	0.0842	0.0849	0.2998	0.0181	0.0200	0.1010	0.0188	0.0191
0.70	0.236	0.3830	0.0839	0.0846	0.3056	0.0180	0.0199	0.1083	0.0190	0.0192
0.70	0.283	0.2666	0.1282	0.1285	0.2878	0.0303	0.0314	0.0851	0.0343	0.0344
0.80	0.185	0.2863	0.0643	0.0652	0.3215	0.0161	0.0185	0.0824	0.0159	0.0162
0.80	0.194	0.3224	0.0772	0.0780	0.3194	0.0184	0.0205	0.0908	0.0182	0.0184
0.80	0.237	0.4243	0.0617	0.0630	0.3160	0.0131	0.0158	0.1175	0.0135	0.0139
0.80	0.245	0.3960	0.0623	0.0633	0.3037	0.0130	0.0156	0.1088	0.0136	0.0140
0.80	0.252	0.6037	0.1796	0.1801	0.3054	0.0295	0.0308	0.1472	0.0299	0.0301
0.80	0.261	0.2579	0.1243	0.1245	0.2912	0.0305	0.0316	0.0776	0.0311	0.0312
0.80	0.269	0.3911	0.0680	0.0687	0.3188	0.0151	0.0176	0.1183	0.0160	0.0164
0.80	0.279	0.3273	0.0688	0.0693	0.3486	0.0181	0.0206	0.1154	0.0196	0.0200
0.80	0.289	0.4226	0.0811	0.0817	0.3642	0.0199	0.0224	0.1479	0.0217	0.0221
0.80	0.353	0.3056	0.1238	0.1240	0.2943	0.0287	0.0299	0.1066	0.0349	0.0350
0.80	0.369	0.2103	0.1236	0.1237	0.3216	0.0358	0.0369	0.0893	0.0453	0.0454
0.90	0.236	0.3871	0.0896	0.0902	0.3293	0.0204	0.0224	0.1119	0.0207	0.0210
0.90	0.325	0.4089	0.0764	0.0770	0.3133	0.0163	0.0185	0.1285	0.0185	0.0189
0.90	0.337	0.4191	0.0830	0.0835	0.2672	0.0149	0.0167	0.1140	0.0172	0.0175
0.90	0.350	0.3033	0.0700	0.0704	0.2433	0.0135	0.0151	0.0838	0.0157	0.0158
0.90	0.435	0.4568	0.1472	0.1475	0.1862	0.0178	0.0185	0.1016	0.0238	0.0240
0.90	0.457	0.2564	0.1262	0.1263	0.1568	0.0169	0.0175	0.0581	0.0236	0.0237
0.90	0.481	0.0549	0.0986	0.0987	0.1431	0.0168	0.0173	0.0142	0.0244	0.0244
0.90	0.509	0.0304	0.1183	0.1183	0.1460	0.0212	0.0216	0.0087	0.0329	0.0329
1.00	0.326	0.3912	0.0696	0.0702	0.3408	0.0166	0.0191	0.1317	0.0184	0.0188
1.00	0.337	0.4124	0.0815	0.0820	0.3456	0.0191	0.0215	0.1412	0.0217	0.0221
1.00	0.389	0.2074	0.1025	0.1027	0.2297	0.0209	0.0219	0.0605	0.0261	0.0262
1.00	0.405	0.2063	0.0969	0.0970	0.2656	0.0229	0.0241	0.0717	0.0294	0.0295
1.00	0.565	0.3706	0.1663	0.1665	0.1612	0.0196	0.0201	0.0926	0.0316	0.0317
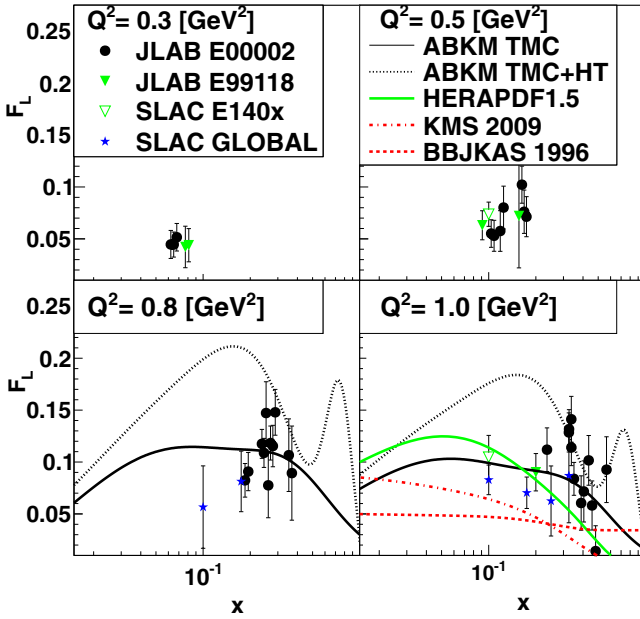
FIG. 4. Proton longitudinal structure-function data for fixed Q^2 as a function of Bjorken x from this experiment. Also shown are data from Jefferson Lab experiment E99–118 [7] and SLAC [2,23]. The four panels correspond to four different Q^2 regions: $Q^2 = 0.3\,\text{GeV}^2$ (upper-left panel), $Q^2 = 0.5\,\text{GeV}^2$ (upper-right panel), $Q^2 = 0.8\,\text{GeV}^2$ (lower-left panel), and $Q^2 = 1.0\,\text{GeV}^2$ (lower-right panel). Also shown are the parametrizations by ABKM [50,51], solid and dotted black curves; HERAPDF1.5 [52], solid green line; KMS [12], dashed-dotted red curves; and BBJKAS [53], dashed red curve.

corrections (TMCs) and higher-twist effects [51]. Therefore, the curves in Fig. 4 include TMCs, both without (solid black line) and with (dotted black line) the inclusion of higher-twist effects. These curves are only shown for the two higher-Q^2 panels because of constraints on the region of validity for the PDF fits.

For the kinematic regime of the Jefferson Lab data, the target-mass corrections and higher-twist effects are expected to be significant, and thus improved agreement is expected with parametrizations that include these effects. However, the ABKM inclusion of higher-twist effects seems to be unnecessary and yields significantly worse agreement with the data. It is important to note also that F_L is dominated by the gluon $g(x)$ PDF, which has large uncertainties ($\sim 20\%$ or more in this x range) that are not shown here.

The PDF fits discussed above utilize the standard collinear factorization formalism. Another approach in modeling F_L is to employ a k_T factorization approach, which corresponds to the (virtual) photon-gluon fusion mechanism. Here, the gluon is off-shell with its virtuality dominated by the transverse momentum k_T [12]. This model (KMS) is shown as a dashed-dotted line at $Q^2 = 1\,\text{GeV}^2$ in Fig. 4. While it undercuts the data, it should be noted that it was developed specifically to describe the low-x, higher-Q^2 regime of data obtained at DESY. An older version of this photon-gluon fusion model [53,54], which specifically included higher-twist effects, is also shown in Fig. 4 (dashed line, BBJKAS) and shows increased
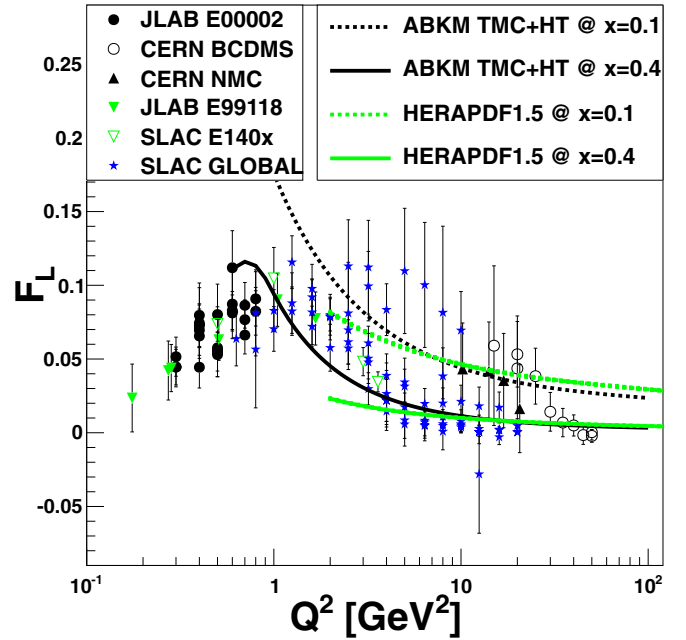

FIG. 5. Longitudinal structure-function data for the proton as a function of Q^2 for $x \geqslant 0.05$. Data are from Refs. [2–4,7,18,23]. The solid and dashed lines represent parametrizations discussed in the text. The dotted lines correspond to $x = 0.1$, while the solid lines correspond to $x = 0.4$.

strength at larger x. A new k_T factorization model that also includes higher twist is in development [55].

In general there is reasonable agreement between the models shown and the data. The global fits typically employ F_2, not F_L, data and extract gluon information from the Q^2 evolution of F_2. Hence, even if deviations between the data and the curves are noticeable, the general agreement at the low Q^2 of the F_L data is unexpected, given that the parametrizations originate from perturbative methods.

To further investigate the Q^2 behavior of the data, we present in Figs. 5 and 6 the world data for F_L versus Q^2 for $x \geqslant 0.05$ (Fig. 5) and for $0.0001 \leqslant x \leqslant 0.006$ (Fig. 6). The data in Fig. 5 were obtained from various experiments at CERN (NMC and BCDMS) and from lower-energy SLAC
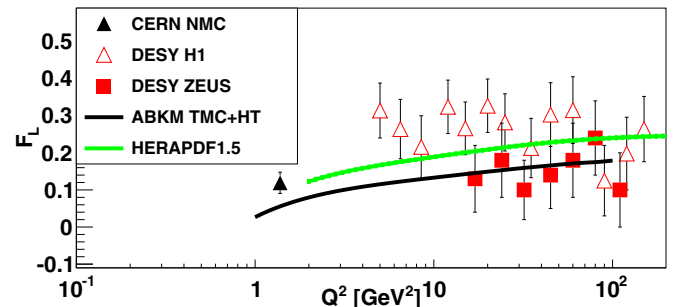

FIG. 6. Proton longitudinal structure-function data at very low x: $0.0001 \leqslant x \leqslant 0.006$ as a function of Q^2. Data are from Refs. [4–6]. The solid lines represent parametrizations discussed in the text and evaluated at $x = 0.004$.

and JLab experiments (E140x, E99–118, and E00–002). The data in Fig. 6 are primarily from the recent DESY H1 and ZEUS experiments [5,6]. In this latter kinematic regime, the longitudinal structure function F_L is dominated by the gluon parton distribution function, and is well described by the PDF parametrizations, which do include these data. The range of the CERN, SLAC, and JLab data (Fig. 5) includes regions where meson-cloud or sea-quark effects may become relevant, as well as the larger-x valence region where nonperturbative binding and other effects may also become relevant, particularly at lower Q^2. The ABKM and HERAPDF fits described previously are also shown in Fig. 5 at $x = 0.1$ and $x = 0.4$ and in Fig. 6 for $x = 0.0004$.

The change in the Q^2 dependence of the higher-x F_L structure-function data from low (<1) to high Q^2 ($> 1 \text{GeV}^2$) that can be seen in Fig. 5 is of particular interest. Due to current conservation, the interaction of longitudinal virtual photons vanishes in the real photon $Q^2 = 0$ limit. Hence, because $\sigma_L \approx F_L/Q^2$, one expects F_L to vanish as Q^4 when $Q^2 \to 0$. This behavior has been used as a kinematic constraint for theoretical modeling [12]. The moderate- to high-x data depicted here were obtained far from the strict real photon $Q^2 = 0$ limit, however, and nonetheless seem to converge smoothly below $Q^2 \approx 1 \text{GeV}^2$ for all x.

In comparison, in the range $1 < Q^2 < 10 \text{GeV}^2$, there is a significant spread to the data. This spread is due largely to the expected x dependence as these data span the range $0.1 \leqslant x \leqslant 0.7$. This spread is predicted also in the global fits at differing values of x. As discussed previously, the nonperturbative effects in the transition to lower Q^2 are overestimated in the ABKM analysis, which regardless agrees reasonably well with the data if the average x is assumed to be 0.4. The average x for the data in the range $0.5 < Q^2 < 5 \text{GeV}^2$ is about 0.2. At the highest values of Q^2, above 10GeV^2, the data once again converge towards 0. Here, the structure function F_L must vanish due to hadron helicity conservation.

V. PROTON-DEUTERON COMPARISON

Lastly, we compare the data accumulated for the deuteron to those for the proton within the Q^2 range accessible to the SLAC and JLab experiments. Inclusive electron scattering experiments such as E00–002 are able to alternately acquire proton and deuteron data, with reduced point-to-point systematic uncertainties in the ratio $R = \sigma_L/\sigma_T$, because some sources of uncertainty are common and therefore vanish in the ratio. It is traditional that Rosenbluth-type measurements present the quantity $R = \sigma_L/\sigma_T$, in part for systematic uncertainty reduction and in part to enable the extraction of cross sections via a variant of Eq. (1):

$$\frac{1}{\Gamma} \frac{d^2\sigma}{d\Omega dE'} = \sigma_T(1 + \varepsilon R). \tag{11}$$

Because ε and R are typically small, σ_T and hence F_1 account for 70–90% of both the cross section and the F_2 structure function. The results for the proton F_2 structure function, the longitudinal structure function F_L, and the ratio R are presented in Table III.
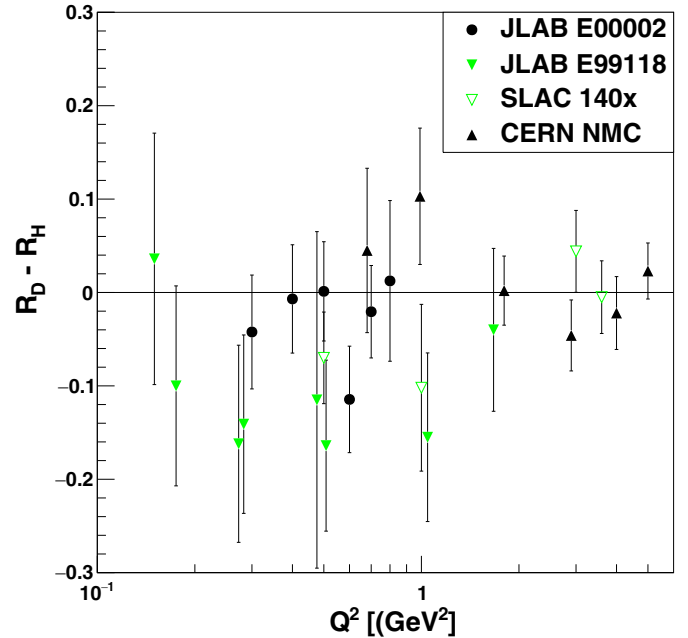

FIG. 7. $R_D - R_H$ as a function of Q^2. The data presented here are above the nucleon resonance region, $W > 2$ GeV.

Figure 7 shows the deuteron-proton difference, $R_D - R_H$, as a function of Q^2, where each point is a weighted average over x of data beyond the nucleon resonance region, $W > 2$ GeV. There is a systematic overall shift of the data towards negative values, indicating that, below $Q^2 = 1.5 \text{GeV}^2$, R for the deuteron may be smaller than that for the proton. For this kinematic range, a weighted average of all available data, including the new E00–002 data, yields $R_D - R_H = -0.042 \pm 0.018$ for $Q^2 < 5 \text{GeV}^2$. This is in agreement with the result obtained by a similar global average presented in Ref. [7], which did not include the present data and obtained $R_D - R_H = -0.054 \pm 0.029$. While this difference is a small quantity, it should be noted that the value of R in this region is on average 0.1, and hence this is a $\geqslant 30\%$ effect.

Measurements of a nuclear dependence of R have been hinted at in the past, most famously by the HERMES Collaboration [56]. However, in this case, no true longitudinal-transverse separation was performed and, in the end, the initially observed effect was attributed dominantly to a background associated with radiative corrections [32].

Although there is nothing to prevent it, there is no theoretical model that predicts the neutron structure-function ratio R_n to differ from the proton R_H. In most previous analyses R_D has been assumed to equal R_H, thus neglecting possible nuclear binding or EMC-effect-type phenomena in the deuteron—or an inherent difference between R_n and R_H. Previous measurements have generally confirmed no difference, i.e., $R_D = R_H$ for $Q^2 \geqslant 1.5$ GeV^2 [2,57]. However, in the high-momentum domain of these measurements, $R_H \approx 0$, and any difference is practically immeasurable at large-Q^2 values. This fact may resolve the apparent discrepancy between the higher-Q^2 results and the results shown here.

TABLE III. Deuterium structure functions R, F_2, and F_L extracted using the Rosebluth separation technique.

| Q^2 (GeV^2)	x	R	Δ_{stat}	Δ_{total}	F_2	Δ_{stat}	Δ_{total}	F_L	Δ_{stat}	Δ_{total}
0.30	0.062	0.2103	0.0669	0.0694	0.2030	0.0115	0.0129	0.0369	0.0106	0.0110
0.30	0.065	0.2141	0.0593	0.0612	0.2039	0.0101	0.0117	0.0377	0.0095	0.0098
0.30	0.068	0.2142	0.0788	0.0799	0.2061	0.0140	0.0151	0.0383	0.0125	0.0127
0.40	0.081	0.2367	0.0639	0.0664	0.2384	0.0124	0.0142	0.0483	0.0118	0.0122
0.40	0.093	0.2890	0.0711	0.0720	0.2420	0.0133	0.0150	0.0584	0.0124	0.0126
0.40	0.097	0.3172	0.1017	0.1023	0.2424	0.0187	0.0199	0.0632	0.0168	0.0169
0.40	0.102	0.3615	0.0976	0.0982	0.2451	0.0170	0.0183	0.0710	0.0156	0.0158
0.40	0.108	0.3062	0.1169	0.1173	0.2448	0.0221	0.0232	0.0632	0.0199	0.0200
0.40	0.114	0.3062	0.1263	0.1266	0.2468	0.0242	0.0252	0.0644	0.0217	0.0218
0.40	0.121	0.3448	0.0584	0.0599	0.2519	0.0109	0.0130	0.0728	0.0100	0.0104
0.50	0.104	0.2608	0.0552	0.0571	0.2642	0.0115	0.0137	0.0588	0.0112	0.0116
0.50	0.108	0.2053	0.0601	0.0613	0.2575	0.0132	0.0152	0.0475	0.0126	0.0128
0.50	0.119	0.2528	0.0833	0.0840	0.2609	0.0177	0.0192	0.0579	0.0166	0.0167
0.50	0.124	0.2869	0.0903	0.0909	0.2651	0.0187	0.0202	0.0655	0.0175	0.0176
0.50	0.163	0.3567	0.0726	0.0733	0.2621	0.0139	0.0158	0.0818	0.0132	0.0135
0.50	0.168	0.3013	0.0738	0.0744	0.2552	0.0148	0.0165	0.0709	0.0143	0.0145
0.50	0.174	0.3775	0.0818	0.0823	0.2601	0.0152	0.0169	0.0865	0.0146	0.0148
0.60	0.127	0.2595	0.0507	0.0519	0.2757	0.0114	0.0139	0.0622	0.0105	0.0108
0.60	0.133	0.2799	0.0523	0.0535	0.2799	0.0116	0.0141	0.0675	0.0109	0.0112
0.60	0.153	0.1833	0.0856	0.0860	0.2660	0.0207	0.0221	0.0469	0.0196	0.0197
0.60	0.161	0.2449	0.0982	0.0985	0.2705	0.0222	0.0236	0.0613	0.0211	0.0212
0.60	0.171	0.3730	0.1223	0.1226	0.2783	0.0240	0.0252	0.0885	0.0232	0.0233
0.70	0.152	0.1894	0.0567	0.0577	0.2774	0.0138	0.0160	0.0493	0.0134	0.0137
0.70	0.158	0.3134	0.0526	0.0536	0.2857	0.0115	0.0141	0.0768	0.0107	0.0110
0.70	0.166	0.2714	0.0545	0.0551	0.2803	0.0124	0.0148	0.0681	0.0116	0.0118
0.70	0.205	0.4366	0.0882	0.0893	0.2804	0.0160	0.0179	0.1032	0.0169	0.0172
0.70	0.214	0.4480	0.2080	0.2082	0.2734	0.0366	0.0374	0.1041	0.0367	0.0368
0.70	0.228	0.2756	0.0799	0.0803	0.2688	0.0175	0.0191	0.0733	0.0178	0.0180
0.70	0.236	0.3779	0.0753	0.0758	0.2712	0.0144	0.0163	0.0952	0.0153	0.0155
0.70	0.283	0.3729	0.1029	0.1032	0.2513	0.0186	0.0199	0.0959	0.0205	0.0207
0.80	0.185	0.3167	0.0726	0.0732	0.2851	0.0156	0.0176	0.0789	0.0152	0.0154
0.80	0.237	0.3768	0.0625	0.0634	0.2768	0.0125	0.0147	0.0946	0.0123	0.0127
0.80	0.245	0.3508	0.0606	0.0613	0.2666	0.0119	0.0141	0.0875	0.0121	0.0124
0.80	0.252	0.4501	0.1384	0.1387	0.2663	0.0239	0.0251	0.1060	0.0241	0.0242
0.80	0.261	0.2945	0.1191	0.1193	0.2605	0.0249	0.0260	0.0770	0.0253	0.0254
0.80	0.269	0.3988	0.0582	0.0589	0.2691	0.0108	0.0132	0.1010	0.0115	0.0118
0.80	0.279	0.3388	0.0591	0.0596	0.2716	0.0119	0.0142	0.0922	0.0130	0.0132
0.80	0.289	0.2823	0.0590	0.0594	0.2642	0.0126	0.0146	0.0795	0.0138	0.0140
0.80	0.353	0.2637	0.0888	0.0890	0.2327	0.0174	0.0186	0.0751	0.0208	0.0209
0.80	0.369	0.2732	0.1002	0.1004	0.2256	0.0188	0.0198	0.0774	0.0233	0.0234
0.90	0.236	0.4082	0.0944	0.0949	0.2842	0.0181	0.0198	0.1003	0.0183	0.0185
0.90	0.325	0.2924	0.0627	0.0630	0.2421	0.0121	0.0139	0.0774	0.0137	0.0138
0.90	0.337	0.1786	0.0571	0.0573	0.2232	0.0120	0.0136	0.0489	0.0138	0.0139
0.90	0.350	0.2688	0.0616	0.0619	0.2200	0.0113	0.0129	0.0690	0.0131	0.0132
0.90	0.435	0.3300	0.1162	0.1164	0.1636	0.0147	0.0154	0.0706	0.0194	0.0195
0.90	0.457	0.3223	0.1259	0.1260	0.1430	0.0141	0.0147	0.0633	0.0194	0.0194
0.90	0.481	0.0950	0.0952	0.0952	0.1357	0.0145	0.0150	0.0224	0.0208	0.0208
0.90	0.509	0.3363	0.1631	0.1632	0.1469	0.0183	0.0188	0.0744	0.0281	0.0282
1.00	0.326	0.3221	0.0753	0.0756	0.2569	0.0148	0.0165	0.0860	0.0163	0.0164
1.00	0.337	0.3511	0.0922	0.0926	0.2507	0.0171	0.0184	0.0912	0.0191	0.0193
1.00	0.389	0.0749	0.0844	0.0845	0.1967	0.0179	0.0188	0.0210	0.0225	0.0226
1.00	0.405	0.2822	0.1031	0.1033	0.2101	0.0172	0.0182	0.0729	0.0224	0.0225
1.00	0.565	0.0923	0.0978	0.0978	0.1432	0.0158	0.0164	0.0257	0.0252	0.0252
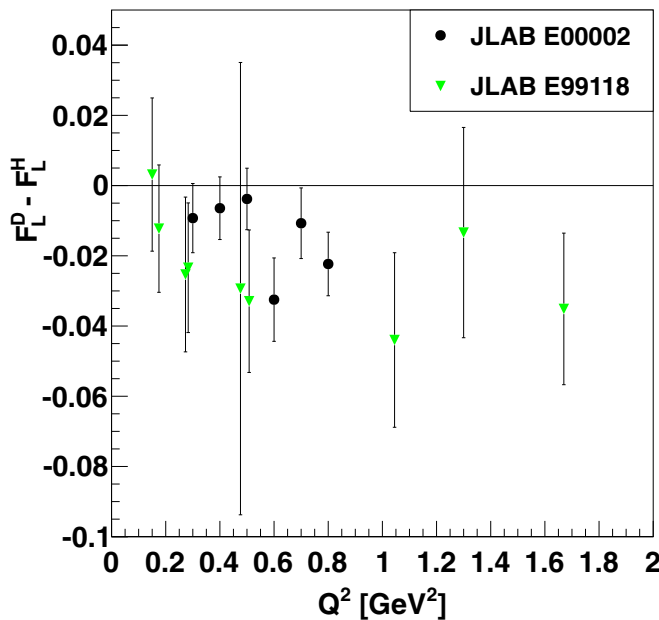
FIG. 8. $F_L^D - F_L^H$ as a function of Q^2.

In the framework of the leading-twist formalism, global QCD fits to available nuclear data allow for enhancements of valence-quark and gluon distributions in nuclei as compared to a free proton [22,58]. The F_L structure function would be uniquely sensitive to such an enhanced gluon distribution [58]. To investigate this possibility, in Fig. 8 we plot the structure function $F_L^D - F_L^H$ as a function of Q^2. The plot shows data from Jefferson Lab experiments E99–118 and E00–002. The SLAC and CERN experiments shown in Fig. 7 do not extract the longitudinal structure function F_L, which is purely a function of the longitudinal cross section, only

the ratio $R = \sigma_L/\sigma_T$. The low-mass deuteron may not be the optimum target for studying gluonic nuclear effects; however, some nuclear dependence of F_L, or perhaps F_L^n differing from F_L^H, is clearly observable in the longitudinal channel at the kinematics accessible here.

VI. CONCLUSION

In conclusion, we report new separated structure-function measurements for hydrogen and deuterium at Q^2 below 2 GeV^2. Available parametrizations and theoretical predictions for the longitudinal structure function F_L describe the data reasonably well when extrapolated to the low-Q^2 and large-x ($0.1 \leqslant x \leqslant 0.6$) kinematics of these new data. Remarkably, the global data set seems to smoothly converge toward zero below $Q^2 = 1.0$ GeV^2, even while it is still far above the current conservation limit. Additionally, the deuterium data seem to confirm a ratio $R = \sigma_L/\sigma_T$ smaller than that of the hydrogen data and therefore indicate either a nuclear dependence of the longitudinal response of the nucleons in the deuteron, and hence a nuclear dependence of the F_L structure function, or a difference between the neutron and proton longitudinal structure functions.

[1] S. Dasu *et al.*, Phys. Rev. D **49**, 5641 (1994).
[2] L. H. Tao *et al.*, Z. Phys. C **70**, 387 (1996).
[3] A. C. Benvenuti *et al.*, Phys. Lett. B **223**, 485 (1989).
[4] M. Arneodo *et al.*, Nucl. Phys. B **483**, 3 (1997).
[5] F. D. Aaron *et al.*, Eur. Phys. J. C **71**, 1579 (2011).
[6] H. Abramowicz *et al.*, Phys. Rev. D **90**, 072002 (2014).
[7] V. Tvaskis *et al.*, Phys. Rev. Lett. **98**, 142301 (2007).
[8] A. Cooper-Sarkar, G. Ingelman, K. R. Long, R. G. Roberts, and D. H. Saxon, Z. Phys. C **39**, 281 (1988).
[9] G. Altarelli and G. Martinelli, Phys. Lett. B **76**, 89 (1978).
[10] G. R. Boroun, Int. J. Mod. Phys. E **18**, 131 (2009).
[11] P. Jimenez-Delgado and E. Reya, Phys. Rev. D **79**, 074023 (2009).
[12] K. Golec-Biernat and A. M. Stasto, Phys. Rev. D **80**, 014006 (2009).
[13] C. Ewerz, A. von Manteuffel, O. Nachtmann, and A. Schoning, Phys. Lett. B **720**, 181 (2013).
[14] G. R. Boroun and B. Rezaei, Eur. Phys. J. C **72**, 2221 (2012).
[15] M. Hentschinski, A. Sabio Vera, and C. Salas, Phys. Rev. D **87**, 076005 (2013).
[16] L. W. Whitlow *et al.*, Phys. Lett. B **250**, 193 (1990).

[17] M. N. Rosenbluth, Phys. Rev. **79**, 615 (1950).
[18] Y. Liang *et al.*, arXiv:nucl-ex/0410027v2; Ph.D. thesis, The American University, 2003.
[19] J. Arrington, F. Coester, R. J. Holt, and T.-S. H. Lee, J. Phys. G **36**, 025005 (2009).
[20] J. Arrington, J. G. Rubin, and W. Melnitchouk, Phys. Rev. Lett. **108**, 252001 (2012).
[21] O. Hen, A. Accardi, W. Melnitchouk, and E. Piasetzky, Phys. Rev. D **84**, 117501 (2011).
[22] A. Accardi, W. Melnitchouk, J. F. Owens, M. E. Christy, C. E. Keppel, L. Zhu, and J. G. Morfín, Phys. Rev. D **84**, 014008 (2011).
[23] L. W. Whitlow *et al.*, Phys. Lett. B **282**, 475 (1992).
[24] S. Malace *et al.*, Phys. Rev. C **80**, 035207 (2009).
[25] M. E. Christy *et al.*, Phys. Rev. C **70**, 015206 (2004).
[26] O. K. Baker *et al.*, Nucl. Instrum. Methods Phys. Res., Sect. A **367**, 92 (1995).
[27] H. Mkrtchyan *et al.*, Nucl. Instrum. Methods Phys. Res., Sect. A **719**, 85 (2013).
[28] D. Abbott *et al.*, Phys. Rev. Lett. **80**, 5072 (1998).
[29] D. Dutta *et al.*, Phys. Rev. C **68**, 064603 (2003).

[30] S. Malace, Ph.D. thesis, Hampton University, 2006, available at https://misportal.jlab.org/ul/generic_reports/hc_thesis.cfm.

[31] V. Tvaskis, Ph.D. thesis, Vrije University, Amsterdam, 2004, available at https://misportal.jlab.org/ul/generic_reports/hc_thesis.cfm.

[32] A. Airapetian *et al.*, Phys. Lett. B **567**, 339(E) (2003).

[33] Y. S. Tsai, Phys. Rev. **122**, 1898 (1961).

[34] L. W. Mo and Y. S. Tsai, Rev. Mod. Phys. **41**, 205 (1969).

[35] D. Y. Bardin *et al.*, Yad. Fiz. **29**, 969 (1979); Nucl. Phys. B **197**, 1 (1982).

[36] S. Dasu *et al.*, Phys. Rev. Lett. **61**, 1061 (1988).

[37] Y. Liang, Ph.D. thesis, American University, 2002, available at https://misportal.jlab.org/ul/generic_reports/hc_thesis.cfm.

[38] M. E. Christy and P. E. Bosted, Phys. Rev. C **81**, 055213 (2010).

[39] P. E. Bosted and M. E. Christy, Phys. Rev. C **77**, 065206 (2008).

[40] J. Arrington, W. Melnitchouk, and J. A. Tjon, Phys. Rev. C **76**, 035205 (2007).

[41] A. J. R. Puckett *et al.*, Phys. Rev. Lett. **104**, 242301 (2010).

[42] A. J. R. Puckett *et al.*, Phys. Rev. C **85**, 045203 (2012).

[43] V. Tvaskis, J. Arrington, M. E. Christy, R. Ent, C. E. Keppel, Y. Liang, and G. Vittorini, Phys. Rev. C **73**, 025206 (2006).

[44] C. E. Carlson and M. Vanderhagen, Annu. Rev. Nucl. Part. Sci. **57**, 171 (2007).

[45] J. Arrington, P. G. Blunden, and W. Melnitchouk, Prog. Part. Nucl. Phys. **66**, 782 (2011).

[46] I. A. Rachek *et al.*, Phys. Rev. Lett. **114**, 062005 (2015).

[47] D. Adikaram *et al.*, Phys. Rev. Lett. **114**, 062003 (2015).

[48] V. Pascalutsa, C. E. Carlson, and M. Vanderhaeghen, Phys. Rev. Lett. **96**, 012301 (2006).

[49] S. Kondratyuk and P. G. Blunden, Nucl. Phys. A **778**, 44 (2006).

[50] S. Alekhin, J. Blumlein, S. Klein, and S. Moch, Phys. Rev. D **81**, 014032 (2010).

[51] S. Alekhin, J. Blumlein, and S. Moch, Phys. Rev. D **86**, 054009 (2012).

[52] H1 and ZEUS Collaborations, preliminary result, available at http://www-h1.desy.de/publications/H1preliminary.short_list.html.

[53] B. Badelek, J. Kwiecinski, and A. Stasto, Z. Phys. C **74**, 297 (1997).

[54] B. Badelek and J. Kwiecinski, Rev. Mod. Phys. **68**, 445 (1996).

[55] A. Stasto (private communication).

[56] K. Ackerstaff *et al.*, Phys. Lett. B **475**, 386 (2000).

[57] M. Arneodo *et al.*, Nucl. Phys. B **487**, 3 (1997).

[58] V. Guzey, L. Zhu, C. E. Keppel, M. E. Christy, D. Gaskell, P. Solvignon, and A. Accardi, Phys. Rev. C **86**, 045201 (2012).